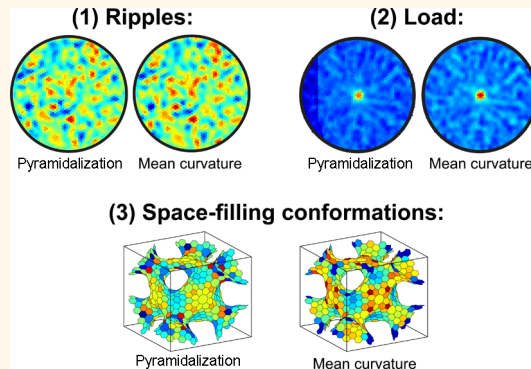


# Quantitative Chemistry and the Discrete Geometry of Conformal Atom-Thin Crystals

Alejandro A. Pacheco Sanjuan,<sup>†,‡</sup> Mehrshad Mehboudi,<sup>†</sup> Edmund O. Harriss,<sup>§</sup> Humberto Terrones,<sup>†</sup> and Salvador Barraza-Lopez<sup>†,\*</sup>

<sup>†</sup>Department of Physics, University of Arkansas, Fayetteville, Arkansas 72701, United States, <sup>‡</sup>Department of Mechanical Engineering, Universidad del Norte, Barranquilla, Colombia, <sup>§</sup>Department of Mathematical Sciences, University of Arkansas, Fayetteville, Arkansas 72701, United States, and <sup>†</sup>Department of Physics and Center for 2-Dimensional and Layered Materials, The Pennsylvania State University, University Park Pennsylvania 16802, United States

**ABSTRACT** When flat or on a firm mechanical substrate, the atomic composition and atomistic structure of two-dimensional crystals dictate their chemical, electronic, optical, and mechanical properties. These properties change when the two-dimensional and ideal crystal structure evolves into arbitrary shapes, providing a direct and dramatic link among geometry and material properties due to the larger structural flexibility when compared to bulk three-dimensional materials. We describe methods to understand the local geometrical information of two-dimensional conformal crystals quantitatively and directly from atomic positions, even in the presence of atomistic defects. We then discuss direct relations among the discrete geometry and chemically relevant quantities—mean bond lengths, hybridization angles, and  $\sigma$ – $\pi$  hybridization. These concepts are illustrated for carbon-based materials and ionic crystals. The pyramidalization angle turns out to be linearly proportional to the mean curvature for relevant crystalline configurations. Discrete geometry provides direct quantitative information on the potential chemistry of conformal two-dimensional crystals.



**KEYWORDS:** conformal geometry · two-dimensional crystals · pyramidalization angle · discrete geometry

The time could not be more ripe to reinvoke the long-standing discussion<sup>1–3</sup> as to how the properties of elastic two-dimensional (2D) conformal elastic crystals<sup>4</sup> are affected by geometry.<sup>5,6</sup> The 2D crystalline membranes adapt to the shape of (*i.e.*, they conform to) harder surfaces,<sup>7–9</sup> develop ripples when freestanding,<sup>10–21</sup> and can be deformed into arbitrary elastic regimes beyond harmonic elasticity theory.<sup>22–27</sup> The field is taking off spectacularly with new materials coming into play and a host of ideas from graphene physics—such as strain engineering<sup>16,17,24–26,28–45</sup>—being applied to other 2D materials with more diverse electronic, valley and spin properties.<sup>46–51</sup> At the present moment, the portfolio of 2D crystals includes graphene,<sup>52–58</sup> hexagonal boron nitride, transition metal dichalcogenides, some oxides,<sup>4,46,59–64</sup> silicene and germanene,<sup>65</sup> and new semiconductor

compounds.<sup>48,49</sup> Their material properties will depend on shape.

Bulk three-dimensional materials cannot exceed a few percent elastic strain. In contrast, freestanding 2D crystals can sustain much larger metric increases and strain into the tens of percent (with or without accompanying curvature); they can be driven away from the harmonic elastic regime with ease.<sup>22,23,66–70</sup> Elastic two-dimensional membranes<sup>71,72</sup> can assume the shape of arbitrary two-dimensional manifolds.<sup>1,73–77</sup> Flexible 2D membranes relieve mechanical in-plane strain originating from defects by buckling out-of-plane, hence trading stretching by bending.<sup>73</sup> The geometry of atomistic membranes can also be determined by the presence of atomistic (topological) defects or lack thereof.<sup>73,78</sup> Atomistic defects also induce radical behavior by localizing electronic orbitals, altering optically available electronic transitions, and can also induce a large curvature and strain.<sup>1,2</sup>

\* Address correspondence to sbarraza@uark.edu.

Received for review December 20, 2013 and accepted January 8, 2014.

Published online January 08, 2014  
10.1021/nn406532z

© 2014 American Chemical Society

When thinking of crystalline membranes, geometry tends to be linked to curvature alone,<sup>1</sup> but when distances among atoms change—even under in-plane strain—the metric changes as well. Since curvature and metric both determine the local geometry, conformations with and without in-plane strain are geometrically distinct already. Furthermore, mechanical strain and metric are directly related and may even be used interchangeably. While mechanical strain may be modeled by a host of mechanical theories, each with their own assumptions (i.e., continuum mechanics through the Cauchy–Born rule<sup>79</sup> versus atomistic mechanics with interatomic potentials,<sup>80</sup> all the way to full *ab initio* based molecular dynamics<sup>81</sup>), one can bypass mechanistic details and couple the relevant optical, electronic, and chemical theories to changes in interatomic distances directly. This concept was pioneered for quantum dots under strain since the late 1980s,<sup>82</sup> and it acquires a renewed relevance for 2D crystals because the structural analysis directly originates from finite atomic displacements, instead of being mediated by a continuum. By progression of thought, these concepts arguably give atomistic (noncontinuum) approaches to geometry a special relevance, too. Those atomistic approaches to geometry are based on meshes,<sup>6,83</sup> but the identification of an abstract mesh with the atomic lattice of 2D crystals is a direct one,<sup>45</sup> and a number of teams are already complementing continuum mechanical<sup>84,85</sup> and electronic structure<sup>16,17,40,45,86</sup> descriptions of crystalline membranes with some decidedly discrete approaches.

We argue that the mathematical tool for geometrical analysis is not just an object to process, filter, and/or fit physical and chemical information. Instead, the geometrical language can in fact lead and motivate the scientific discussion. This observation is particularly acute regarding chemistry. Within continuum geometry/elasticity theory, a 2D membrane is a chemically inert atom-less medium, and no discussion of chemical reactivity (or aromaticity for carbon-based materials) has ever originated from within continuum elasticity as far as we know.

On the other hand, consider as an example benzene-like carbon materials (such as graphene), where *aromaticity* is a structural property.<sup>87</sup> Infinite ideal 2D graphene has three equivalent aromatic Clar structures that lead to a constant mean bond length (MBL) (Figure 1a).<sup>87–98</sup> This is identical to say that the metric (Figure 1c) is constant in such a system, thus suggesting an intimate connection among aromatic behavior and geometry. Now that the link among the aromaticity of carbon rings and the metric has been exposed, the next interesting and related question from a chemical perspective is: What is the reactivity/aromaticity of strain-engineered graphene?<sup>29–31,33</sup> As far as we know, this question is yet to be addressed; the issue of chemical reactivity under nonplanar structural conformations will

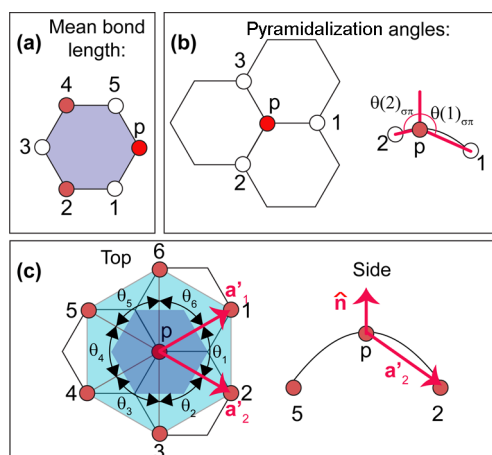


**Figure 1.** Atoms required to determine local chemical measures and the geometrical parameters in eqs 1–3 and 5–7 for 2D crystals with hexagonal structure and no buckling. (a) Atoms required to determine mean bond lengths on a hexagon. (b) Four atoms needed to determine pyramidalization angles. (c) Local lattice displacements  $a_1$  and  $a_2$ , internal angles  $\theta_i$  to edges  $e_i$  and  $e_{i+1}$ , and darker shaded hexagon of area  $A_p$  are shown; side view shows the normal vector  $\hat{n}$ .

certainly become more relevant as the science of conformal 2D crystals continues to be explored in years to come.

Now, relevant for orbital hybridization,<sup>43</sup> spin–orbit coupling,<sup>99,100</sup> and chemical reactivity, the pyramidalization angle<sup>101</sup>  $\alpha_{\text{pyr}}$  relates to the angular deviation among the local normal and bond vectors (Figure 1b). The fact that curvature (obtained from points in Figure 1c) and  $\alpha_{\text{pyr}}$  could be related may be expected intuitively, but their explicit dependence has not been discussed so far. Their explicit relation will be one of the main results of this paper.

Hence, we argue by example that geometry originating from atoms is a powerful concept leading to new scientific perspectives, new intuition, and to precise yet intuitive links to potential chemical and physical phenomena. In addition, although the systems discussed here explicitly are carbon-based, the general ideas are expected to apply for many 2D crystals because the discussion here is of a general character as it pertains to geometry. Most of the phenomena at the single-electron level have to be explainable by (i) chemical composition, (ii) electron orbital symmetries,<sup>102–105</sup> (iii) thermodynamics,<sup>106,107</sup> and other dynamical information at the relevant electron energies. Geometry is a control handle for these properties.

The geometrical analysis applies unchanged to graphene, nanotubes,<sup>2,102,108–123</sup> single-layer hexagonal boron nitride,<sup>46</sup> and novel crystals with nonbuckled hexagonal structure as those discussed by Hennig recently.<sup>48,49</sup> The formalism is then extended by means of approximations to study arbitrary two-dimensional nanomaterials with more general shapes, such as fullerenes,<sup>124–129</sup> Schwarzes,<sup>130</sup> ionic crystals,<sup>78,131–133</sup>

and other hexagonal systems with atomistic defects. Thicker conformal systems (such as single-layer transition metal dichalcogenides or 2D systems with other than hexagonal lattices) could be later explored along similar lines.

**Chemical Measures and Structure.** Three measures originate from carbon-based materials.

(1) Mean bond length (MBL): Aromaticity is not a directly measurable property, and hence it cannot be defined unambiguously. Yet, the structure accommodating the maximum number of Clar sextets best represents chemical and physical properties, and Clar sextet migration increases chemical reactivity. How aromatic is conformal graphene?<sup>18</sup> Can rippling be explained in terms of the creation of “aromatic domains”? The MBL is defined as follows (Figure 1a):<sup>87,94</sup>

$$\text{MBL} = \bar{a}_{CC} = \frac{1}{6} \sum_{i=1}^6 a_{CC,i} \quad (1)$$

where  $a_{CC,i}$  are bond lengths on a closed loop as depicted in Figure 1a. According to ref 94, MBL is a reliable tool for analysis of large aromatic systems. To reach this conclusion, they compared their results with the pseudo- $\pi$  method<sup>134</sup> in the context of the six-center bond index (SCI) analysis on graphene nanoribbons.

(2) The angle  $\theta_{\sigma\pi}$  between the bonds and the normal vector  $\hat{\mathbf{n}}$  at atom p has a single value  $\theta_{\sigma\pi}$  under a spherical geometry<sup>101</sup> and  $\theta_{\sigma\pi} = \pi/2$  on a flat surface. The  $\theta_{\sigma\pi}$  can be generalized for arbitrary geometries as an average:

$$\bar{\theta}_{\sigma\pi} \equiv \frac{1}{3} \sum_{i=1}^3 \theta(i)_{\sigma\pi} \quad (2)$$

with  $\theta(i)_{\sigma\pi}$  being the angle among a bond vector and the local normal (Figure 1b). Equation 2 takes its usual form for fullerenes, where  $\theta(i)_{\sigma\pi} = \theta_{\sigma\pi}$  for all bonds.<sup>101</sup> The pyramidalization angle  $\alpha_{\text{pyr}}$  is defined by Haddon<sup>101</sup> as follows:

$$\alpha_{\text{pyr}} = \bar{\theta}_{\sigma\pi} - \pi/2 \quad (3)$$

(3) The  $\sigma-\pi$  orbital hybridization: In the presence of curvature, the hopping parameter  $t$  between nearest neighbors (1 and 2) for materials with s and p electrons is modified to include hybridization among  $\sigma$  and  $\pi$  electrons, as follows:<sup>43</sup>

$$t \rightarrow (\hat{n}_1 \cdot \hat{r})(\hat{n}_2 \cdot \hat{r})(t_\sigma + \delta t_\sigma) + [\hat{n}_1 - (\hat{n}_1 \cdot \hat{r})\hat{r}] \cdot [\hat{n}_2 - (\hat{n}_2 \cdot \hat{r})\hat{r}](t + \delta t) \quad (4)$$

where  $\hat{n}_1$  and  $\hat{n}_2$  are local normals for atoms 1 and 2,  $\mathbf{r}$  is the vector joining them, and  $\hat{r} = \mathbf{r}/r$ . For example, for a planar 2D crystal  $\hat{n}_1$  and  $\hat{n}_2$  are orthogonal to  $\hat{r}$ , and  $t \rightarrow t + \delta t$  (i.e., there is no  $\sigma-\pi$  hybridization), as expected. The effect of  $\sigma-\pi$  electron coupling tends to be small, and it is sometimes neglected but it is important to visualize the magnitude of the coupling coefficient  $(\hat{n}_1 \cdot \hat{r})(\hat{n}_2 \cdot \hat{r})$  in relevant atomistic conformations.

We next discuss geometry of atomic crystals in a comprehensive way.

#### Local Geometry of Two-Dimensional Elastic Membranes from Atomic Positions.

The local geometry of two-dimensional surfaces is determined from their metric ( $g$ ) and curvature ( $k$ ) in terms of four invariants that indicate how the two-dimensional manifold stretches and curves along two directions with respect to a reference non-deformed configuration. Given two in-plane vector fields  $\mathbf{g}_1$  and  $\mathbf{g}_2$ , a well-defined metric  $g_{\alpha\beta} \equiv \mathbf{g}_\alpha \cdot \mathbf{g}_\beta$  must be symmetric ( $g_{\alpha\beta} = g_{\beta\alpha}$ ) and positive definite ( $g_{\alpha\alpha} > 0$ )<sup>135</sup> ( $\alpha, \beta = 1, 2$ ). Then, the four invariant geometrical measures are (i)  $\det(g) = |\mathbf{g}_1|^2 |\mathbf{g}_2|^2 - |\mathbf{g}_1 \cdot \mathbf{g}_2|^2$ ,  $\text{Tr}(g) = \sum_{\alpha=1}^2 |\mathbf{g}_\alpha|^2$ , the Gauss curvature  $K \equiv \det(k)/\det(g)$ , and  $H \equiv \sum_{\alpha=1}^2 k_{\alpha\alpha}/2g_{\alpha\alpha}$  the mean curvature. (In a continuum approach, the curvature is derived from the metric tensor as follows:  $k_{\alpha\beta} = \hat{\mathbf{n}} \cdot (\partial \mathbf{g}_\alpha / \partial \xi^\beta)$  with  $\xi^\beta$  an in-plane coordinate. See, e.g., ref 136.)

Two-dimensional conformal crystals can be studied with nontraditional tools that include discrete geometry, discrete differential geometry (DDG), and discrete exterior calculus. Classical, *Riemannian* differential geometry studies the properties of smooth, continuum objects, and *discrete* geometry studies geometrical shapes made of polyhedra. DDG, in turn, seeks discrete equivalents of notions and methods of continuous and discrete geometry and applies to conformal 2D crystals transparently. In fact, many concepts of smooth geometry are limiting procedures of discretizations. The main points for DDG are that interatomic distances determine the discretization limit, and that the continuum limit is not granted on atomistic meshes. As seen in the next section, both curvatures can be expressed within the framework of DDG.

## RESULTS

**Basic Framework.** Discrete geometry is expressed from atomic positions, and the discrete metric is defined from lattice displacements  $\mathbf{a}'_\alpha$ <sup>16,17,45</sup> on the deformed lattice (Figure 1c):

$$g_{\alpha\beta} = \mathbf{a}'_\alpha \cdot \mathbf{a}'_\beta \quad (5)$$

The Gauss curvature ( $K$ ) originates from the angle defect  $\sum_{i=1}^6 \theta_i$  (Figure 1c) as follows:<sup>6,83,137</sup>

$$K = (2\pi - \sum_{i=1}^6 \theta_i)/A_p \quad (6)$$

where  $\theta_i$  ( $i = 1, \dots, 6$ ) are inner angles among vertices and the *Voronoi tessellation* (darker blue in Figure 1c) encloses the area  $A_p$  of a unit cell. Consistent with the existence of two atoms on the unit cell of 2D crystals with hexagonal symmetry,<sup>46,48,56</sup> the points  $p$  and 1–6 in Figure 1c belong to the same sublattice. On a flat surface, for example, the angle defect adds up to  $2\pi$ , making  $K = 0$ , as expected.

Still relying on Figure 1c for geometrical guidance, the mean curvature  $H$  averages the relative orientations of edges and normal vectors along a closed path, and it is a signed quantity (i.e., it is sensitive to the side of the 2D surface through its projection onto the local normal  $\hat{\mathbf{n}}$ ):

$$H = \frac{\sum_{i=1}^6 \mathbf{e}_i \times (\mathbf{v}_{i,i+1} - \mathbf{v}_{i-1,i})}{4A_p} \cdot \hat{\mathbf{n}} \quad (7)$$

Here,  $\mathbf{v}_i$  is the position of atom  $i$  on sublattice  $A$ ,  $\mathbf{e}_i = \mathbf{v}_i - \mathbf{v}_p$  is the edge between points  $p$  and  $i$  (note that  $\mathbf{a}_{1(2)} = \mathbf{e}_{1(2)}$ );  $\mathbf{v}_{i,i+1}$  is the normal to edges  $\mathbf{e}_i$  and  $\mathbf{e}_{i+1}$  ( $i$  is a cyclic index), and  $\hat{\mathbf{n}} = (\sum_{i=1}^6 \mathbf{v}_{i,i+1} A_i) / (\sum_{i=1}^6 A_i)$  is the area-weighted normal with  $A_i = |\mathbf{e}_i \times \mathbf{e}_{i+1}| / 2$ .<sup>6,45</sup> (See ref 45 for extensive discussion.) The mean curvature can enhance the spin-orbit coupling in carbon-based nanomaterials.<sup>99,100</sup>

**Additional Remarks on Exponential Maps.** On the discrete geometry, one never leaves the atomistic membrane because all quantities are expressed in terms of actual atomic positions. On continuum approaches to mechanics/geometry, on the other hand, it is quite possible that tangents lie outside of the 2D manifold, and this must be remediated. The well-known Cauchy–Born rule applies to space-filling materials but not to crystalline membranes, unless corrected with an exponential map (Figure 2).<sup>45,136,138–140</sup> The acute need for exponential maps becomes yet another difference among 2D conformal crystals and bulk 3D materials. The need for exponential maps is not a technical matter but a fundamental geometrical requirement for geodesic curves in 2D manifolds. Exponential maps are deeply rooted and long-known for the geometrical description of surfaces<sup>5,135,141</sup> and must be enforced onto descriptions of nanoscale phenomena in conformal crystalline membranes.

## DISCUSSION

**Relations among Chemical Measures and the Discrete Local Geometry.** Even though the relation among mean bond lengths and metric is direct, the degree of sensitivity of MBL with respect to fluctuations on interatomic distances makes a direct correlation difficult.<sup>16–18</sup> In Figure 3a–c, we contrast MBL with  $\text{Tr}(g)$  and  $\det(g)$  (we will not display the determinant of the metric tensor in other figures; see ref 45 for extensive discussion). Details of the creation of the rippled structure can be found in prior work<sup>16,17,45</sup> (see Methods section, too). Recalling the notion that pristine graphene has equal bond lengths, Figure 3a indicates that atomistic fluctuations will have a bearing on the aromatic behavior of rippled samples; this concept, or its ramifications, has not been discussed before. Further analysis requires specific theoretical tools beyond our reach (see ref 134). [Here we mention that the

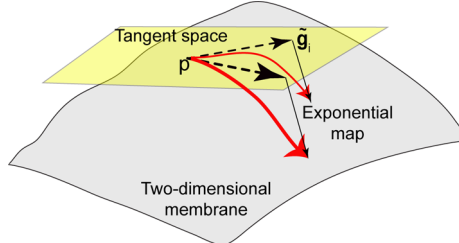


Figure 2. In three-dimensional materials, a deformation field always belongs to the bulk. In 2D conformal crystals, on the other hand, a continuum deformation field may lie outside of the material body. Structural stability requires redefining the standard Cauchy–Born rule,<sup>79</sup> so that deformations are mapped back into the two-dimensional material. Being defined onto the atomistic membrane, discrete geometry does not require such a mapping.

structure was obtained at 1 K (see Methods). At this temperature, the lattice constant is on the order of 1.39 Å, but we use the more common value of 1.41 Å when normalizing; the metric in Figure 3b,c reflects this normalization.]

There exists a remarkably simple one-to-one correlation among the pyramidalization angle and the mean curvature (sign included) for all of the systems studied, as already evident from Figure 3d,e. Put simply, we find

$$\alpha_{\text{pyr}} (\text{in rads}) \approx 1 \times H (\text{in } \text{\AA}^{-1}) \quad (8)$$

Equation 8 is an interesting result because it gives a commonly used angular measure for orbital hybridization and chemical reactivity a simple geometrical character. This result will hold for other hexagonal 2D crystals and deserves additional discussion.

The  $\alpha_{\text{pyr}}$  is a signed quantity, as follows: Direct inspection of Figure 1b and eq 3 indicates that  $\alpha_{\text{pyr}}$  will be positive for a bulge and negative for a sag. Similarly, the mean curvature  $H$  in eq 7 is a vector quantity projected onto the local normal; the relative orientation of the normal (facing “up” or “down”) confers  $H$  with a sign, as well. (Geometrically speaking, one sees that radius of curvature changes sign for a bulge or a sag, so  $H$  must in fact be signed.) However, the correspondence goes beyond the sign. The cross products on  $H$  (eq 7) confer an additional sinusoidal function, which approximates as the angle rather well up to 20° (0.35 rad), which is within the range of all pyramidalization angles seen in this work. The correlation on display in eq 8 is remarkable as it informs our intuition concerning hybridization, thus making the mean curvature a direct tool for analysis of hybridization and chemical reactivity for 2D systems with s and p electrons.

Now, the coefficient  $(\hat{\mathbf{n}}_1 \cdot \hat{\mathbf{r}})(\hat{\mathbf{n}}_2 \cdot \hat{\mathbf{r}})$  in eq 4 approximates the amount of  $\sigma$  mixing onto  $\pi$  electrons in graphene and renormalizes the Fermi velocity in that system. Here we see that its magnitude is negligible ( $10^{-4}$ ) for this sample of rippled graphene (Figure 3f). (It may be worth mentioning here the existence of a

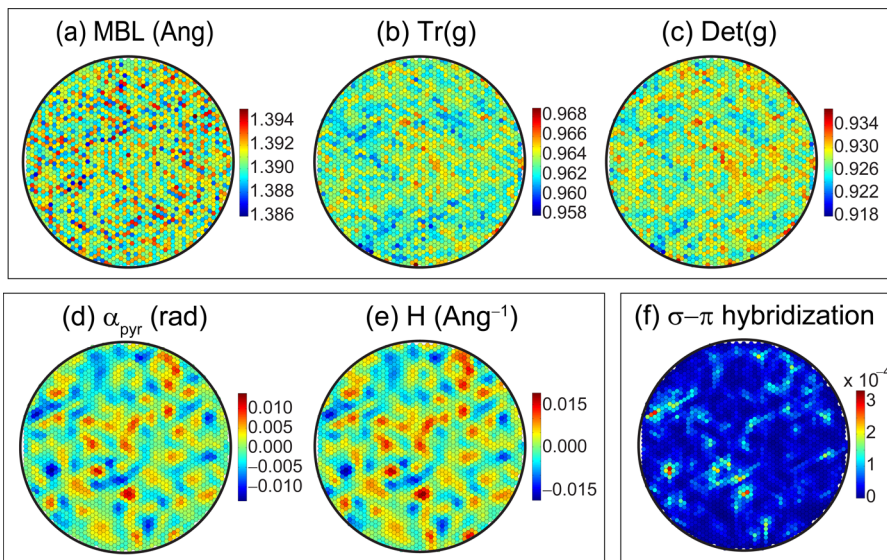


**Figure 3. Chemical measures and the local geometry of a rippled 2D crystal with hexagonal symmetry. While no direct correlation can be drawn among MBL in (a) and metric measures in (b,c), the pyramidalization  $\alpha_{\text{pyr}}$  in (d) is directly proportional to the mean curvature  $H$  in (e); this holds for all systems studied; (f)  $\sigma$ – $\pi$  mixing<sup>43</sup> is small ( $\sim 10^{-4}$ ).**

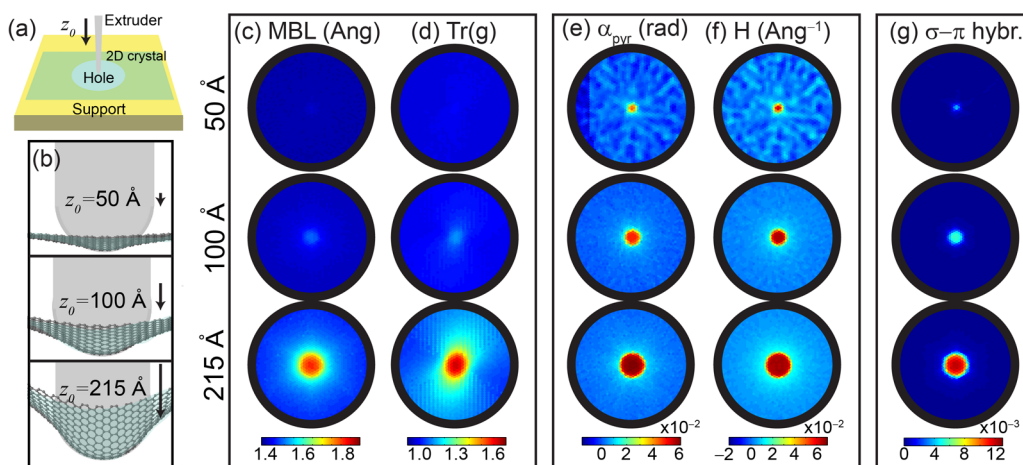


**Figure 4. Chemical measures and the local geometry of a rippled 2D crystal with hexagonal symmetry under mechanical load.**

roughly quadratic relation among  $H$  and this coefficient, which is not pursued further.)

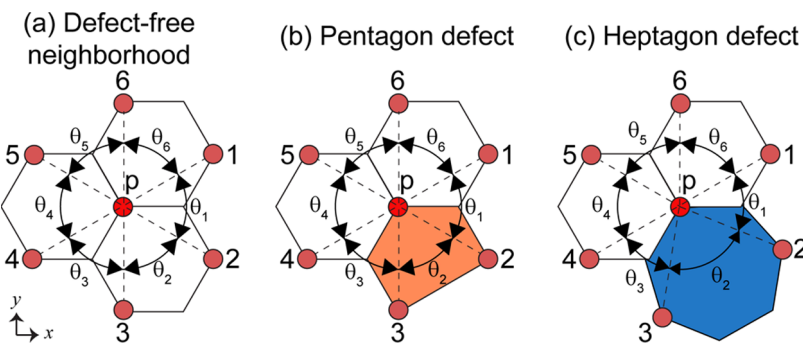
Let us next consider these geometrical and chemical measures when the 2D membrane in Figure 3 is under mechanical load. We worked with a large sample containing a few million atoms, and extensive technical details have been given before.<sup>16,17,45</sup> Let us concentrate on geometrical aspects relevant to chemistry next.

Figure 4a provides basic schematics of the mechanical indentation procedure: The 2D crystal is held fixed outside the central circular region, and a spherical extruder pushes the 2D membrane down. Data are analyzed at indentation heights of 50, 100, and 215 Å (Figure 4b). To highlight atomistic detail, the same area was employed as in Figure 3. The discrete metric is formed by the lattice vectors on the deformed manifold, which are not orthogonal. This shows in Figure 4d, which lacks spherical symmetry.<sup>45</sup> Nevertheless, the indentation

ironed out the ripples seen in Figure 3 before indentation, and this helps develop a one-to-one relation among MBL and  $\text{Tr}(g)$  (Figure 4c,d). Note interatomic distances as big as 1.8 Å, well beyond the harmonic elastic regime.<sup>16</sup>

Interestingly, the relation among  $\alpha_{\text{pyr}}$  and  $H$  still remains, and  $H$  (Figure 4f) reproduces all and every single detail from  $\alpha_{\text{pyr}}$  (Figure 4e), even though they are obtained following very different premises (eq 1 versus eq 7). Even under extreme mechanical load, the coefficient  $(\hat{n}_1 \cdot \hat{r})(\hat{n}_2 \cdot \hat{r})$  in eq 4 (Figure 4g) is still smaller than a few percent, an encouraging result as it grants a sound footing to the effective theories of massless fermions in graphene in terms of  $\pi$  electrons only, even under such rather strong mechanical deformation.<sup>45</sup>

**Atomistic Defects and Mixed (Atomistic/Continuum) Approaches to the Geometry of 2D Conformal Crystals.** The pentagon (heptagon) defect in Figure 5b will furnish a positive (negative) Gauss curvature  $K$ . The presence



**Figure 5.** Neighborhood of an atom changes upon appearance of topological defects. (a) Neighborhood with no topological defects (see Figure 1c). The more common defects are (b) a pentagon defect, (c) a heptagon defect, or a combination of (b) and (c). Although the curvatures can still be obtained for a (b) and (c) by considering the atoms shown in red, the discrete metric breaks down, and a continuum metric is given by interpolation methods.

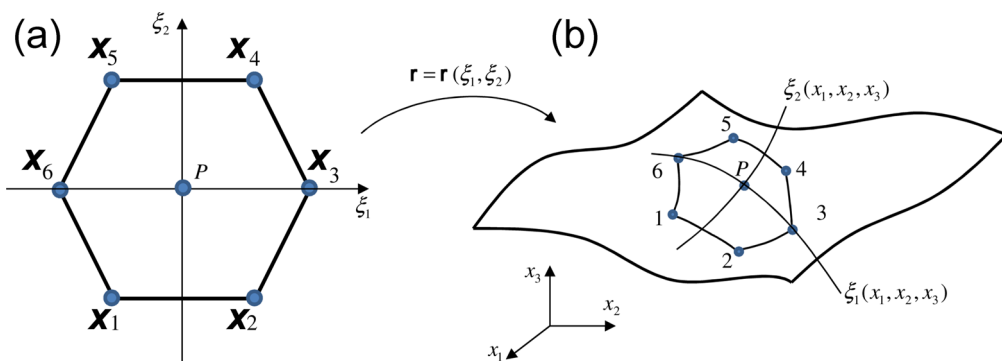


**Figure 6.** (a) Orthogonal two-dimensional convective coordinate set ( $\xi^1, \xi^2$ ) and a polygon. (b) Deformed polygon on an actual 2D crystal. Partial derivatives, necessary in defining the continuum metric, are taken on the convective space.

of defects therefore leads to an infinite variety of structures. Topological defects break the crystal symmetry, and the crystalline metric (eq 5) will not be well-defined around atomistic defects. Hence, we develop next a metric in terms of continuous, differentiable vector fields that interpolate atomic positions.

Incidentally, this discussion is quite relevant at this moment, and it finds a unique place within the context of continuum formalism for “strain-engineering” of 2D crystals<sup>16,17,24–26,28–45,50,86</sup> as it presents with clarity “black-box” details of continuum approximations from atomistic meshes which have not been discussed up to this point. The specific approach presented here relies on the atomic lattice; it works with and without defects and constitutes another ingredient of novelty on the present article. (Care must be exercised in that atomistic defects play the fundamental and non-negligible role of (pseudo)magnetic monopole sources on the effective electron theories for carbon-based materials.<sup>142</sup>)

In the approach presented here, all nodal points originate from atoms. This approach, appropriately called *conforming polygonal*, is employed nowadays for structural analysis.<sup>143</sup> Consider a point  $p$  with coordinates  $(\xi^1, \xi^2)$  inside the regular polygon on the plane in Figure 6a and the polygon with the same number of sides formed by  $n_p$  atoms and coordinates  $\mathbf{r}_i = (x_i, y_i, z_i)$  ( $i = 1, \dots, n_p$ ) on the conformal 2D crystal (Figure 6b). A point with

continuum coordinates  $\mathbf{r} = (x, y, z)$  inside the conformal 2D crystal (Figure 6b) is found by interpolation:

$$\mathbf{r} = \sum_{i=1}^{n_p} \mathbf{r}_i \phi_i(\xi^1, \xi^2) \quad (9)$$

and the continuum metric is expressed from vector fields in terms of the (convective) coordinates  $(\xi^1, \xi^2)$ :

$$\mathbf{g}_\alpha = \frac{\partial \mathbf{r}}{\partial \xi^\alpha} \text{ and } g_{\alpha\beta} = \mathbf{g}_\alpha \cdot \mathbf{g}_\beta \quad (\alpha, \beta = 1, 2) \quad (10)$$

This process is carried out at each polygon in the sample, and the metric displayed in Figures 7 and 8 was evaluated at each polygon’s center. The (Laplace) interpolating (shape) functions in eq 9 are defined by

$$\phi_i(\xi^1, \xi^2) = \frac{w_i(\xi^1, \xi^2)}{\sum_{j=1}^{n_p} w_j(\xi^1, \xi^2)} \quad (11)$$

with  $w_i$  a function of areas  $A$  given in terms of three points defining the polygon on the convective space (Figure 6a):

$$w_i(\xi^1, \xi^2) = \frac{A(\mathbf{x}_{i-1}, \mathbf{x}_i, \mathbf{x}_{i+1})}{A(\mathbf{x}_{i-1}, \mathbf{x}_i, (\xi^1, \xi^2)) \times A(\mathbf{x}_i, \mathbf{x}_{i+1}, (\xi^1, \xi^2))} \quad (12)$$

We keep this discussion short; extensive information is given in ref 143.

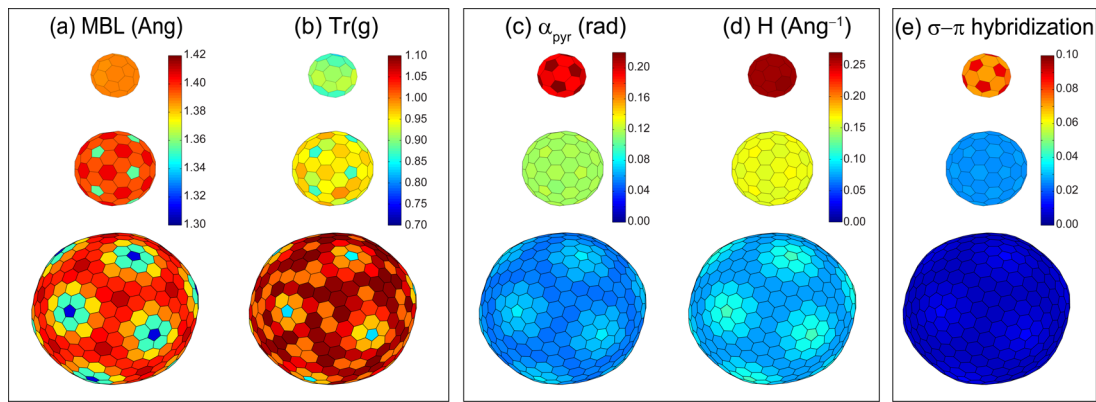


Figure 7. Chemical and geometrical measures for three ionic crystals.<sup>78</sup>

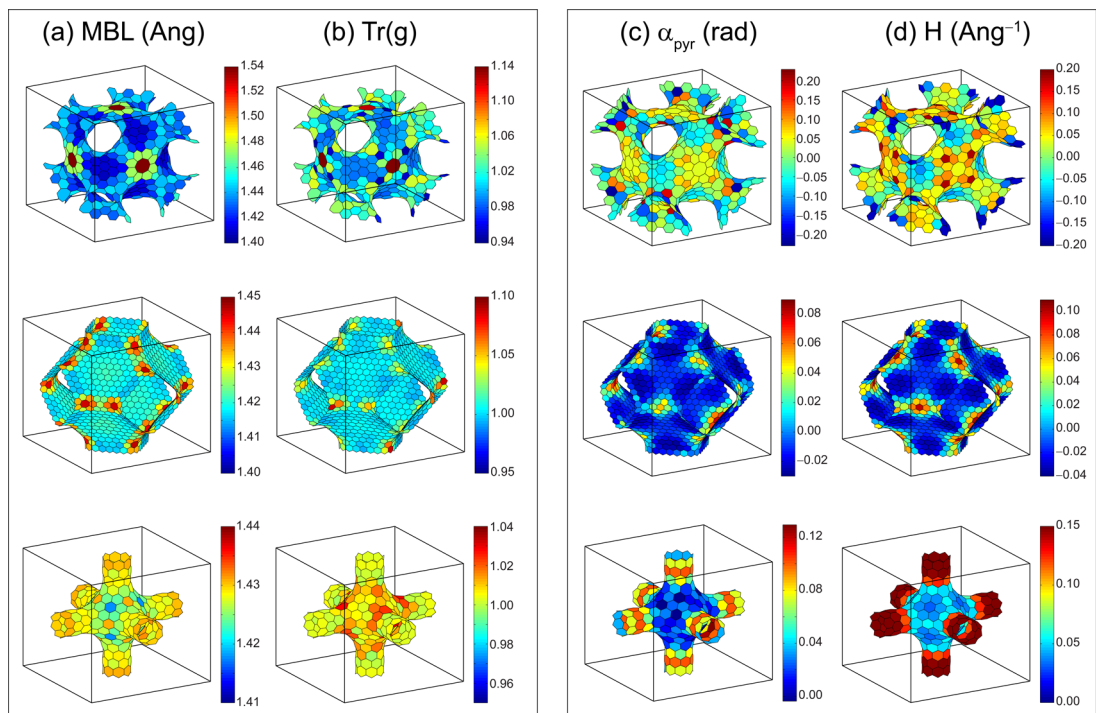


Figure 8. Chemical and geometrical measures for three space-filling 2D crystalline materials.

We have just indicated that we will be approximating the metric to discuss surfaces with topological defects, but curvature must be dealt with additional care. Deep-ingrained perceptions from continuum geometry, such as a curvature evolving smoothly from point to point, break down in crystalline surfaces, where *discrete objects* (atoms and bonds) concentrate and *carry all curvature*.<sup>6</sup> For this fundamental reason, we express curvature in systems with atomistic defects from the six points highlighted in Figure 5, still employing eqs 5 and 6 to extract geometrical information, thus carrying on with the discrete approach to curvature even in the presence of atomistic defects. We display in Figures 7 and 8 the chemical relevant measures and the local geometry for a host of interesting structures with topological defects. All relations found for 2D

crystals with no defects, and discussed in Figures 3 and 4, continue to hold.

**Additional Remarks on Kinetics and Thermodynamics.** In considering the kinetics and thermodynamics of two-dimensional crystals, energy barriers to atomic rearrangements may also depend on shape.<sup>106,107,144</sup> Thus, the geometry discussed here—in terms of atoms alone—may prove very useful in establishing quantitative connections among shape, kinetics and thermodynamics. These connections may prove essential, for example, to study potential growth mechanisms of 2D crystals on conformal geometry.

## CONCLUSION

We proposed in the recent past a discrete theory for Dirac fermions on graphene and soon found the need

to explore the geometrical framework in which these theories rest. As the family of 2D atomic crystals (graphene, hexagonal boron nitride, silicene, germanene, novel binary semiconductors) and (layered) transition metal dichalcogenides and topological insulators continues to grow, establishing atom-based geometrical tools for analysis of the properties of these 2D systems (both graphene and beyond graphene) is a justified and current endeavor.

By their dimensionality, 2D crystals can sustain large deformations, well beyond the reach of continuum elasticity theory. In addition, continuum elasticity only works in the bulk, as in 2D crystals a continuum deformation field may lie outside of the material body.

We exemplify the discrete geometry and uncover a linear relation among a chemically relevant measure (piramidalization angle) and a fundamental geometrical measure (mean curvature). In spite of the longevity of the field of atom-thin materials, such insightful

identification has never been discussed before, and it may become useful for chemical insights as the field continues to evolve with ever greater vigor.

The concepts were illustrated on a number of carbon-based systems under rippling, mechanical load, on ionic crystals with spherical symmetry and on some other crystalline structures including Schwarzsites. Those concepts will translate effortlessly into other 2D crystals.

We also discussed ways to merge continuum and discrete approaches for analysis of 2D conformal crystals. By explaining the nuts and bolts of such approaches, we decisively contribute to the discussion of continuum frameworks and atomistic approaches to uncover the properties of 2D crystals. Geometry from atoms is a concept relevant to chemistry, and it will have an impact on better informing our intuition regarding the chemical properties of 2D crystals with shape, an area of research experiencing a renewed thrust.

## METHODS

The structures generated to study rippling—created by line stress at the edges—and mechanical load were obtained from molecular dynamics<sup>80</sup> of a 3 million atom (finite) graphene square patch with no periodic boundary conditions in thermal equilibrium at 1 K. The geometrical study focused on a small patch near the geometrical center.

*Conflict of Interest:* The authors declare no competing financial interest.

*Acknowledgment.* We thank NSF-XSEDE TACC's Stampede (Grant TG-PHY090002) and Arkansas (Razor II) for computational support.

*Note Added after ASAP Publication:* After publication on January 13, 2014 and due to a production error, a minor typographical correction was made to a label in Figure 4. Data was not affected. The revised version was reposted on January 28, 2014.

## REFERENCES AND NOTES

- Lord, E. A.; Mackay, A. L.; Ranganathan, S. *New Geometries for New Materials*, 1st ed.; Cambridge University Press: Cambridge, 2006.
- Saito, R.; Dresselhaus, G.; Dresselhaus, M. S. *Physical Properties of Carbon Nanotubes*, 1st ed.; Imperial College Press: London, 1998.
- Dresselhaus, M. S.; Terrones, M. Carbon-Based Nanomaterials from a Historical Perspective. *Proc. IEEE* **2013**, *101*, 1522–1535.
- Novoselov, K. S.; Jiang, D.; Schedin, F.; Booth, T. J.; Khotkevich, V. V.; Morozov, S. V.; Geim, A. K. Two-Dimensional Atomic Crystals. *Proc. Natl. Acad. Sci. U.S.A.* **2005**, *102*, 10451–10453.
- Kühnel, W. *Differential Geometry*, 1st ed.; American Mathematical Society: Providence, RI, 2002.
- Sullivan, J. M. In *Discrete Differential Geometry*, 1st ed.; Bobenko, A. I., Schröder, P., Sullivan, J. M., Ziegler, G. M., Eds.; Oberwolfach Seminars; Springer: Berlin, 2008; Vol. 38.
- Morozov, S.; Novoselov, K.; Katsnelson, M.; Schedin, F.; Ponomarenko, L.; Jiang, D.; Geim, A. Strong Suppression of Weak Localization in Graphene. *Phys. Rev. Lett.* **2006**, *97*, 016801.
- Mohanty, N.; Nagaraja, A.; Fahrenholz, M.; Boyle, D.; Berry, V. Impermeable Graphenic Encasement of Bacteria. *Nano Lett.* **2011**, *11*, 1270–1275.
- Yamamoto, M.; Pierre-Louis, O.; Huang, J.; Fuhrer, M.; Einstein, T.; Cullen, W. The Princess and the Pea at the Nanoscale: Wrinkling and Delamination of Graphene on Nanoparticles. *Phys. Rev. X* **2012**, *2*, 041018.
- Meyer, J. C.; Geim, A. K.; Katsnelson, M. I.; Novoselov, K. S.; Booth, T. J.; Roth, S. The Structure of Suspended Graphene Sheets. *Nature* **2007**, *446*, 60–63.
- Tapaszto, L.; Dumitrica, T.; Kim, S. J.; Nemes-Incze, P.; Hwang, C.; Biro, L. P. Breakdown of Continuum Mechanics for Nanometre-Wavelength Rippling of Graphene. *Nat. Phys.* **2012**, *8*, 739–742.
- Shenoy, V. B.; Reddy, C. D.; Ramasubramaniam, A.; Zhang, Y. W. Edge-Stress-Induced Warping of Graphene Sheets and Nanoribbons. *Phys. Rev. Lett.* **2008**, *101*, 245501.
- Huang, B.; Liu, M.; Su, N.; Wu, J.; Duan, W.; Gu, B.-L.; Liu, F. Quantum Manifestations of Graphene Edge Stress and Edge Instability: A First-Principles Study. *Phys. Rev. Lett.* **2009**, *102*, 166404.
- Wang, H.; Upmanyu, M. Rippling Instabilities in Suspended Nanoribbons. *Phys. Rev. B* **2012**, *86*, 205411.
- Vandeparre, H.; Piñeirua, M.; Brau, F.; Roman, B.; Bico, J.; Gay, C.; Bao, W.; Lau, C. N.; Reis, P. M.; Damman, P. Wrinkling Hierarchy in Constrained Thin Sheets from Suspended Graphene to Curtains. *Phys. Rev. Lett.* **2011**, *106*, 224301.
- Sloan, J. V.; Pacheco Sanjuan, A. A.; Wang, Z.; Horvath, C.; Barraza-Lopez, S. Strain Gauge Fields for Rippled Graphene Membranes under Central Mechanical Load: An Approach beyond First-Order Continuum Elasticity. *Phys. Rev. B* **2013**, *87*, 155436.
- Barraza-Lopez, S.; Pacheco Sanjuan, A. A.; Wang, Z.; Vanević, M. Strain-Engineering of Graphene's Electronic Structure Beyond Continuum Elasticity. *Solid State Commun.* **2013**, *166*, 70–75.
- Fasolino, A.; Los, J. H.; Katsnelson, M. I. Intrinsic Ripples in Graphene. *Nat. Mater.* **2007**, *6*, 858–861.
- Zakharchenko, K.; Roldán, R.; Fasolino, A.; Katsnelson, M. Self-Consistent Screening Approximation for Flexible Membranes: Application to Graphene. *Phys. Rev. B* **2010**, *82*, 125435.
- Zakharchenko, K. V.; Katsnelson, M. I.; Fasolino, A. Finite Temperature Lattice Properties of Graphene beyond the Quasiharmonic Approximation. *Phys. Rev. Lett.* **2009**, *102*, 046808.
- Gibertini, M.; Tomadin, A.; Polini, M.; Fasolino, A.; Katsnelson, M. I. Electron Density Distribution and Screening in Rippled Graphene Sheets. *Phys. Rev. B* **2010**, *81*, 125437.

22. Lee, C.; Wei, X.; Kysar, J. W.; Hone, J. Measurement of the Elastic Properties and Intrinsic Strength of Monolayer Graphene. *Science* **2008**, *321*, 385–388.
23. Lee, G.-H.; Cooper, R. C.; An, S. J.; Lee, S.; van der Zande, A.; Petrone, N.; Hammerberg, A. G.; Lee, C.; Crawford, B.; Oliver, W.; *et al.* High-Strength Chemical-Vapor-Deposited Graphene and Grain Boundaries. *Science* **2013**, *340*, 1073–1076.
24. Levy, N.; Burke, S. A.; Meaker, K. L.; Panlasigui, M.; Zettl, A.; Guinea, F.; Castro-Neto, A. H.; Crommie, M. F. Strain-Induced Pseudo-magnetic Fields Greater Than 300 T in Graphene Nanobubbles. *Science* **2010**, *329*, 544–547.
25. Klimov, N. N.; Jung, S.; Zhu, S.; Li, T.; Wright, C. A.; Solaras, S. D.; Newell, D. B.; Zhitenev, N. B.; Stroscio, J. A. Electromechanical Properties of Graphene Drumheads. *Science* **2012**, *336*, 1557–1561.
26. Xu, P.; Yang, Y.; Barber, S. D.; Ackerman, M. L.; Schoelz, J. K.; Qi, D.; Kornev, I. A.; Dong, L.; Bellachia, L.; Barraza-Lopez, S.; *et al.* Atomic Control of Strain in Freestanding Graphene. *Phys. Rev. B* **2012**, *85*, 121406(R).
27. Eder, F. R.; Kotakoski, J.; Holzweber, K.; Mangler, C.; Skakalova, V.; Meyer, J. C. Probing from Both Sides: Reshaping the Graphene Landscape via Face-to-Face Dual-Probe Microscopy. *Nano Lett.* **2013**, *13*, 1934–1940.
28. Suzuura, H.; Ando, T. Phonons and Electron–Phonon Scattering in Carbon Nanotubes. *Phys. Rev. B* **2002**, *65*, 235412.
29. Pereira, V. M.; Castro-Neto, A. H. Strain Engineering of Graphene’s Electronic Structure. *Phys. Rev. Lett.* **2009**, *103*, 046801.
30. Guinea, F.; Katsnelson, M. I.; Geim, A. K. Energy Gaps and a Zero-Field Quantum Hall Effect in Graphene by Strain Engineering. *Nat. Phys.* **2010**, *6*, 30–33.
31. Vozmediano, M. A. H.; Katsnelson, M. I.; Guinea, F. Gauge Fields in Graphene. *Phys. Rep.* **2010**, *496*, 109–148.
32. de Juan, F.; Cortijo, A.; Vozmediano, M. A. H. Charge Inhomogeneities Due To Smooth Ripples in Graphene Sheets. *Phys. Rev. B* **2007**, *76*, 165409.
33. de Juan, F.; Cortijo, A.; Vozmediano, M. A. H.; Cano, A. Aharonov-Bohm Interferences from Local Deformations in Graphene. *Nat. Phys.* **2011**, *7*, 810–815.
34. de Juan, F.; Sturla, M.; Vozmediano, M. A. H. Space Dependent Fermi Velocity in Strained Graphene. *Phys. Rev. Lett.* **2012**, *108*, 227205.
35. de Juan, F.; Mañes, J. L.; Vozmediano, M. A. H. Gauge Fields from Strain in Graphene. *Phys. Rev. B* **2013**, *87*, 165131.
36. Kitt, A. L.; Pereira, V. M.; Swan, A. K.; Goldberg, B. B. Erratum: Lattice-Corrected Strain-Induced Vector Potentials in Graphene [Phys. Rev. B 85, 115432 (2012)]. *Phys. Rev. B* **2013**, *87*, 159909(E).
37. Neek-Amal, M.; Covaci, L.; Peeters, F. M. Nanoengineered Nonuniform Strain in Graphene Using Nanopillars. *Phys. Rev. B* **2012**, *86*, 041405(R).
38. Masir, M. R.; Peeters, D. M.; Pseudo, F. M. Magnetic Field in Strained Graphene: Revisited. *Solid State Commun.* **2013**, *175–176*, 76–82.
39. Moldovan, D.; Ramezani Masir, M.; Peeters, F. M. Electronic States in a Graphene Flake Strained by a Gaussian Bump. *Phys. Rev. B* **2013**, *88*, 035446.
40. Neek-Amal, M.; Covaci, L.; Shakouri, K.; Peeters, F. M. Electronic Structure of a Hexagonal Graphene Flake Subjected to Triaxial Stress. *Phys. Rev. B* **2013**, *88*, 115428.
41. Kerner, R.; Naumis, G. G.; Gómez-Arias, W. A. Bending and Flexural Phonon Scattering: Generalized Dirac Equation for an Electron Moving in Curved Graphene. *Physica B* **2012**, *407*, 2002–2008.
42. Oliva-Leyva, M.; Naumis, G. G. Understanding Electron Behavior in Strained Graphene as a Reciprocal Space Distortion. *Phys. Rev. B* **2013**, *88*, 085430.
43. Mañes, J. L.; de Juan, F.; Sturla, M.; Vozmediano, M. A. H. Generalized Effective Hamiltonian for Graphene under Nonuniform Strain. *Phys. Rev. B* **2013**, *88*, 155405.
44. Hicks, J.; Tejeda, A.; Taleb-Ibrahimi, A.; Nevius, M. S.; Wang, F. F.; Shepperd, K. K.; Palmer, J. J.; Bertran, F.; Le Févre, P.; Kunc, J.; *et al.* A Wide-Bandgap Metal-Semiconductor-Metal Nanostructure Made Entirely from Graphene. *Nat. Phys.* **2013**, *9*, 49–54.
45. Pacheco Sanjuan, A. A.; Wang, Z.; Pour-Imani, H.; Vanević, M.; Barraza-Lopez, S. Graphene’s Morphology and Electronic Properties from Discrete Differential Geometry. Submitted for publication.
46. Jin, C.; Lin, F.; Suenaga, K.; Iijima, S. Fabrication of a Freestanding Boron Nitride Single Layer and Its Defect Assignments. *Phys. Rev. Lett.* **2009**, *102*, 195505.
47. Geim, A. K.; Grigorieva, I. V. van der Waals Heterostructures. *Nature* **2013**, *499*, 419–425.
48. Zhuang, H. L.; Hennig, R. G. Computational Discovery of Single-Layer CdO for Electronic Applications. *Appl. Phys. Lett.* **2013**, *103*, 212102.
49. Zhuang, H. L.; Singh, A. K.; Hennig, R. G. Computational Discovery of Single-Layer III–V Materials. *Phys. Rev. B* **2013**, *87*, 165415.
50. Castellanos-Gómez, A.; Roldán, R.; Capelluti, E.; Buschema, M.; Guinea, F.; van der Zant, H. S. J.; Steele, G. A. Local Strain Engineering in Atomically Thin MoS<sub>2</sub>. *Nano Lett.* **2013**, *13*, 5361–5366.
51. Butler, S. Z.; Hollen, S. M.; Cao, L.; Cui, Y.; Gupta, J. A.; Gutiérrez, H. R.; Heinz, T. F.; Hong, S. S.; Huang, J.; Ismach, A. F.; *et al.* Progress, Challenges, and Opportunities in Two-Dimensional Materials beyond Graphene. *ACS Nano* **2013**, *7*, 2898–2926.
52. Wallace, P. The Band Theory of Graphite. *Phys. Rev.* **1947**, *71*, 622–634.
53. McClure, J. W. Energy Band Structure of Graphite. *IBM J. Res. Dev.* **1964**, *8*, 255–261.
54. Semenoff, G. W. Condensed Matter Simulation of a Three-Dimensional Anomaly. *Phys. Rev. Lett.* **1984**, *53*, 2449–2452.
55. DiVincenzo, D. P.; Mele, E. J. Self Consistent Effective Mass Theory for Intralayer Screening in Graphite Intercalation Compounds. *Phys. Rev. B* **1984**, *29*, 1685–1694.
56. Novoselov, K. S.; Geim, A. K.; Morozov, S. V.; Jiang, D.; Katsnelson, M. I.; Grigorieva, I. V.; Dubonos, S. V.; Firsov, A. A. Two-Dimensional Gas of Massless Dirac Fermions in Graphene. *Nature* **2005**, *438*, 197–200.
57. Zhang, Y.; Tan, Y.-W.; Stormer, H. L.; Kim, P. Experimental Observation of the Quantum Hall Effect and Berry’s Phase in Graphene. *Nature* **2005**, *438*, 201–204.
58. Castro Neto, A. H.; Guinea, F.; Peres, N. M. R.; Novoselov, K. S.; Geim, A. K. The Electronic Properties of Graphene. *Rev. Mod. Phys.* **2009**, *81*, 109–162.
59. Wang, Q. H.; Kalantar-Zadeh, K.; Kis, A.; Coleman, J. N.; Strano, M. S. Electronics and Optoelectronics of Two-Dimensional Transition Metal Dichalcogenides. *Nat. Nanotechnol.* **2012**, *7*, 699–712.
60. Mak, K. F.; Lee, C.; Hone, J.; Shan, J.; Heinz, T. F. Atomically Thin MoS<sub>2</sub>: A New Direct-Gap Semiconductor. *Phys. Rev. Lett.* **2010**, *105*, 136805.
61. Zhan, Y.; Liu, Z.; Najmaei, S.; Ajayan, P. M.; Lou, J. Large-Area Vapor-Phase Growth and Characterization of MoS<sub>2</sub> Atomic Layers on a SiO<sub>2</sub> Substrate. *Small* **2012**, *8*, 966–971.
62. Lee, Y. H.; Zhang, X. Q.; Zhang, W.; Chang, M. T.; Lin, C. T.; Chang, K. D.; Yu, Y. C.; Wang, J. T.; Chang, C. S.; Li, L. J.; *et al.* Synthesis of Large-Area MoS<sub>2</sub> Atomic Layers with Chemical Vapor Deposition. *Adv. Mater.* **2012**, *24*, 2320–2325.
63. Gutierrez, H. R.; Perea-Lopez, N.; Elias, A. L.; Berkdemir, A.; Wang, B.; Lv, R.; Lopez-Urias, F.; Crespi, V. H.; Terrones, H.; Terrones, M. Extraordinary Room-Temperature Photoluminescence in Triangular WS<sub>2</sub> Monolayers. *Nano Lett.* **2013**, *13*, 3447–3454.
64. Lin, L.; Xu, Y.; Zhang, S.; Ross, I. M.; Ong, A. C. M.; Allwood, D. A. Fabrication of Luminescent Monolayered Tungsten Dichalcogenides Quantum Dots with Giant Spin-Valley Coupling. *ACS Nano* **2013**, *7*, 8214–8223.
65. Cahangirov, S.; Topsakal, M.; Aktürk, E.; Sahin, H.; Ciraci, S. Two- and One-Dimensional Honeycomb Structures of Silicon and Germanium. *Phys. Rev. Lett.* **2009**, *102*, 236804.

66. He, K.; Poole, C.; Mak, K. F.; Shan, J. Experimental Demonstration of Continuous Electronic Structure Tuning via Strain in Atomically Thin MoS<sub>2</sub>. *Nano Lett.* **2013**, *13*, 2931–2936.

67. Zhao, W.; Ribeiro, R. M.; Toh, M.; Carvalho, A.; Kloc, C.; Castro Neto, A. H.; Eda, G. Origin of Indirect Optical Transitions in Few-Layer MoS<sub>2</sub>, WS<sub>2</sub>, and WSe<sub>2</sub>. *Nano Lett.* **2013**, *13*, 5627–5634.

68. Lee, G.-H.; Yu, Y.-J.; Cui, X.; Petrone, N.; Lee, C.-H.; Choi, M. S.; Lee, D.-Y.; Lee, C.; Yoo, W. J.; Watanabe, K.; et al. Flexible and Transparent MoS<sub>2</sub> Field-Effect Transistors on Hexagonal Boron Nitride–Graphene Heterostructures. *ACS Nano* **2013**, *7*, 7931–7936.

69. Hui, Y. Y.; Liu, X.; Jie, W.; Chan, N. Y.; Hao, J.; Hsu, Y.-T.; Li, L.-J.; Guo, W.; Lau, S. P. Exceptional Tunability of Band Energy in a Compressively Strained Trilayer MoS<sub>2</sub> Sheet. *ACS Nano* **2013**, *7*, 7126–7131.

70. Conley, H. J.; Wang, B.; Ziegler, J. I.; Haglund, R. F., Jr.; Pantelides, S. T.; Bolotin, K. I. Bandgap Engineering of Strained Monolayer and Bilayer MoS<sub>2</sub>. *Nano Lett.* **2013**, *13*, 3626–3630.

71. Nelson, D. R. *Defects and Geometry in Condensed Matter Physics*; Cambridge University Press: Cambridge, 2002.

72. Nelson, D. R.; Weinberg, S.; Piran, T. *Statistical Mechanics of Membranes and Surfaces*; World Scientific: Singapore, 2004.

73. Seung, H.; Nelson, D. Defects in Flexible Membranes with Crystalline Order. *Phys. Rev. A* **1988**, *38*, 1005–1018.

74. Terrones, H.; Mackay, A. L. The Geometry of Hypothetical Curved Graphite Structures. *Carbon* **1992**, *30*, 1251–1260.

75. Terrones, H.; Mackay, A. L. Triply Periodic Minimal Surfaces Decorated with Curved Graphite. *Chem. Phys. Lett.* **1993**, *207*, 45–50.

76. Hyde, S.; Andersson, S.; Larsson, K.; Blum, Z.; Landh, T.; Lidin, S.; Ninham, B. W.; Mackay, A. L. The Language of Shape: The Role of Curvature in Condensed Matter. *Nature* **1997**, *387*, 249–249.

77. Terrones, H.; Terrones, M.; López-Urias, F.; Rodriguez-Manzo, J. A.; Mackay, A. L. Shape and Complexity at the Atomic Scale: The Case of Layered Nanomaterials. *Philos. Trans. A Math. Phys. Eng. Sci.* **2004**, *362*, 2039–2063.

78. Wales, D. J.; McKay, H.; Altschuler, E. L. Defect Motifs for Spherical Topologies. *Phys. Rev. B* **2009**, *79*, 224115.

79. Landau, L. D.; Lifshitz, E. M. *Theory of Elasticity*, 3rd ed.; Elsevier Science: Amsterdam, 1986.

80. Plimpton, S. Fast Parallel Algorithms for Short-Range Molecular Dynamics. *J. Comput. Phys.* **1995**, *117*, 1–19. <http://lammps.sandia.gov>.

81. Car, R.; Parrinello, M. Unified Approach for Molecular Dynamics and Density-Functional Theory. *Phys. Rev. Lett.* **1985**, *55*, 2471–2474.

82. Pryor, C.; Kim, J.; Wang, L. W.; Williamson, A. J.; Zunger, A. Comparison of Two Methods for Describing the Strain Profiles in Quantum Dots. *J. Appl. Phys.* **1998**, *83*, 2548–2554.

83. Xu, Z.; Xu, G. Discrete Schemes for Gaussian Curvature and Their Convergence. *Comp. Math. Appl.* **2009**, *57*, 1187–1195.

84. Ariza, M. P.; Ortiz, M. Discrete Dislocations in Graphene. *J. Mech. Phys. Solids* **2010**, *58*, 710–734.

85. Ariza, M. P.; Serrano, R.; Mendez, J. P.; Ortiz, M. Stacking Faults and Partial Dislocations in Graphene. *Philos. Mag.* **2012**, *92*, 2004–2021.

86. Qi, Z.; Bahamon, D. A.; Pereira, V. M.; Park, H. S.; Campbell, D. K.; Castro Neto, A. H. Resonant Tunneling in Graphene Pseudomagnetic Quantum Dots. *Nano Lett.* **2013**, *13*, 2692–2697.

87. Wu, D.; Gao, X.; Zhou, Z.; Chen, Z. Understanding Aromaticity of Graphene and Graphene Nanoribbons by the Clar Sextet Rule. In *Graphene Chemistry: Theoretical Perspectives*; Jian, D., Chen, Z., Eds.; John Wiley and Sons: New York, 2013; Chapter 3, pp 29–49.

88. Randić, M. Aromaticity of Polycyclic Conjugated Hydrocarbons. *Chem. Rev.* **2003**, *103*, 3449–3606.

89. Wassmann, T.; Seitsonen, A. P.; Marco Saitta, A.; Lazzeri, M.; Mauri, F. Structure, Stability, Edge States, and Aromaticity of Graphene Ribbons. *Phys. Rev. Lett.* **2008**, *101*, 096402.

90. Ormsby, J.; King, B. Clar Valence Bond Representation of p-Bonding in Carbon Nanotubes. *J. Org. Chem.* **2004**, *69*, 4287–4291.

91. Matsuo, Y.; Tahara, K.; Nakamura, E. Theoretical Studies on Structures and Aromaticity of Finite-Length Armchair Carbon Nanotubes. *Org. Lett.* **2003**, *5*, 3181–3184.

92. Baldoni, M.; Sgamellotti, A.; Mercuri, F. Electronic Properties and Stability of Graphene Nanoribbons: An Interpretation Based on Clar Sextet Theory. *Chem. Phys. Lett.* **2008**, *464*, 202–207.

93. Wassmann, T.; Seitsonen, A.; Saitta, A.; Lazzeri, M.; Mauri, F. Clar's Theory, STM Images, and Geometry of Graphene Nanoribbons. *J. Am. Chem. Soc.* **2010**, *132*, 3440–3451.

94. Martin-Martinez, F.; Fias, S.; van Lier, G.; De Proft, F.; Geerlings, P. Electronic Structure and Aromaticity of Graphene Nanoribbons. *Chem.—Eur. J.* **2012**, *18*, 6183–6194.

95. Popov, I.; Bozhenko, K.; Boldyrev, A. Is Graphene Aromatic? *Nano Res.* **2012**, *5*, 117–123.

96. Fuji, S.; Enoki, T. Clar's Aromatic Sextet and  $\pi$ -Electron Distribution in Nanographene. *Angew. Chem., Int. Ed.* **2012**, *51*, 7236–7241.

97. Gutman, I.; Tomović, Z.; Müllen, K.; Rabe, J. On the Distribution of  $\pi$ -Electrons in Large Polycyclic Aromatic Hydrocarbons. *Chem. Phys. Lett.* **2004**, *397*, 412–416.

98. Petersen, R.; Pedersen, T.; Jauho, A. Clar Sextet Analysis of Triangular, Rectangular, and Honeycomb Graphene Antidot Lattices. *ACS Nano* **2011**, *5*, 523–529.

99. Ando, T. Spin–Orbit Interaction in Carbon Nanotubes. *J. Phys. Soc. Jpn.* **2000**, *69*, 1757–1763.

100. Huertas-Hernando, D.; Guinea, F.; Brataas, A. Spin–Orbit Coupling in Curved Graphene, Fullerenes, Nanotubes, and Nanotube Caps. *Phys. Rev. B* **2006**, *74*, 155426.

101. Haddon, R. C. Chemistry of the Fullerenes: The Manifestation of Strain in a Class of Continuous Aromatic Molecules. *Science* **1993**, *261*, 1545–1550.

102. White, C. T.; Mintmire, J. W. Density of States Reflects Diameter in Nanotubes. *Nature* **1998**, *394*, 29–30.

103. Lopez-Bezanilla, A.; Campos-Delgado, J.; Sumpter, B. G.; Baptista, D. L.; Hayashi, T.; Kim, Y. A.; Muramatsu, H.; Endo, M.; Achete, C. A.; Terrones, M.; et al. Geometric and Electronic Structure of Closed Graphene Edges. *J. Phys. Chem. Lett.* **2012**, *3*, 2097–2102.

104. Dyer, C.; Driva, P.; Sides, S. W.; Sumpter, B. G.; Mays, J. W.; Chen, J.; Kumar, R.; Goswami, M.; Dadmun, M. D. Effect of Macromolecular Architecture on the Morphology of Polystyrene–Polyisoprene Block Copolymers. *Macromolecules* **2013**, *46*, 2023–2031.

105. Romo-Herrera, J. M.; Terrones, M.; Terrones, H.; Meunier, V. Guiding Electrical Current in Nanotube Circuits Using Structural Defects: A Step Forward in Nanoelectronics. *ACS Nano* **2008**, *2*, 2585–2591.

106. Kumeda, Y.; Wales, D. J. *Ab Initio* Study of Rearrangements between C<sub>60</sub> Fullerenes. *Chem. Phys. Lett.* **2003**, *374*, 125–131.

107. McKay, H.; Wales, D. J.; Jenkins, S. J.; Verges, J. A.; de Andres, P. L. Hydrogen on Graphene under Stress: Molecular Dissociation and Gap Opening. *Phys. Rev. B* **2010**, *81*, 075425.

108. Iijima, S. Helical Microtubules of Graphitic Carbon. *Nature* **1991**, *354*, 56–58.

109. Iijima, S.; Ajayan, P. M.; Ichihashi, T. Growth Model for Carbon Nanotubes. *Phys. Rev. Lett.* **1992**, *69*, 3100–3103.

110. Ebbesen, T. W.; Ajayan, P. M. Large-Scale Synthesis of Carbon Nanotubes. *Nature* **1992**, *358*, 220–222.

111. Oberlin, A.; Endo, M. Filamentous Growth of Carbon through Benzene Decomposition. *J. Cryst. Growth* **1976**, *32*, 335–349.

112. Terrones, M. Synthesis, Properties, and Applications of Carbon Nanotubes. *Annu. Rev. Mater. Res.* **2003**, *33*, 419–501.

113. Saito, R.; Fujita, M.; Dresselhaus, G.; Dresselhaus, M. S. Electronic Structure of Chiral Graphene Tubules. *Appl. Phys. Lett.* **1992**, *60*, 2204.

114. Odom, T. W.; Huang, J.-L.; Kim, P.; Lieber, C. M. Atomic Structure and Electronic Properties of Single-Walled Carbon Nanotubes. *Nature* **1998**, *391*, 62–64.

115. Wildoer, J. W. G.; Venema, L. C.; Rinzler, A. G.; Smalley, R. E.; Dekker, C. Electronic Structure of Atomically Resolved Carbon Nanotubes. *Nature* **1998**, *391*, 59–62.

116. Iijima, S.; Ichihashi, T. Single-Shell Carbon Nanotubes of 1-nm Diameter. *Nature* **1993**, *363*, 603–605.

117. Jorio, A.; Saito, R.; Hafner, J. H.; Lieber, C. M.; Hunter, M.; McClure, T.; Dresselhaus, G.; Dresselhaus, M. S. Structural (*n,m*) Determination of Isolated Single-Wall Carbon Nanotubes by Resonant Raman Scattering. *Phys. Rev. Lett.* **2001**, *86*, 1118–1121.

118. Arnold, M. S.; Green, A. A.; Hulvat, J. F.; Stupp, S. I.; Hersam, M. C. Sorting Carbon Nanotubes by Electronic Structure Using Density Differentiation. *Nat. Nanotechnol.* **2006**, *1*, 60–65.

119. Liu, H.; Nishide, D.; Tanaka, T.; Kataura, H. Large-Scale Single-Chirality Separation of Single-Wall Carbon Nanotubes by Simple Gel Chromatography. *Nat. Commun.* **2011**, *2*, 309.

120. Mintmire, J. W.; Dunlap, B. I.; White, C. T. Are Fullerene Tubules Metallic? *Phys. Rev. Lett.* **1992**, *68*, 631–634.

121. Mintmire, J. W.; White, C. T. Universal Density of States for Carbon Nanotubes. *Phys. Rev. Lett.* **1998**, *81*, 2506–2509.

122. Cabria, I.; Mintmire, J. W.; White, C. T. Metallic and Semiconducting Narrow Carbon Nanotubes. *Phys. Rev. B* **2003**, *67*, R121406.

123. White, C. T.; Mintmire, J. W. Fundamental Properties of Single-Wall Carbon Nanotubes. *J. Phys. Chem. B* **2005**, *109*, 52–65.

124. Kroto, H. W.; Heath, J. R.; O'Brien, S. C.; Curl, R. F.; Smalley, R. E.  $C_{60}$ : Buckminsterfullerene. *Nature* **1985**, *318*, 162–163.

125. Krätschmer, W.; Lamb, L. D.; Fostiropoulos, K.; Huffman, D. R. Solid  $C_{60}$ : A New Form of Carbon. *Nature* **1990**, *347*, 354–358.

126. Taylor, R.; Hare, J. P.; Abdul-Sada, A. K.; Kroto, H. W. Isolation, Separation and Characterisation of the Fullerenes  $C_{60}$  and  $C_{70}$ : The Third Form of Carbon. *J. Chem. Soc., Chem. Commun.* **1990**, *20*, 1423–1425.

127. Stephens, P. W.; Mihaly, L.; Lee, P. L.; Whetten, R. L.; Huang, S.-M.; Kaner, R.; Deiderich, F.; Holczer, K. Structure of Single-Phase Superconducting  $K_3C_{60}$ . *Nature* **1991**, *351*, 632–634.

128. David, W. I. F.; Ibberson, R. M.; Matthewman, J. C.; Prassides, K.; Dennis, T. J. S.; Hare, J. P.; Kroto, H. W.; Taylor, R.; Walton, D. R. M. Crystal Structure and Bonding of Ordered  $C_{60}$ . *Nature* **1991**, *353*, 147–149.

129. Dresselhaus, M. S.; Dresselhaus, G.; Eklund, P. C. *Science of Fullerenes and Carbon Nanotubes*; Academic Press: San Diego, CA, 1996.

130. Terrones, H.; Terrones, M.; Hsu, W. K. Beyond  $C_{60}$ : Graphite Structures for the Future. *Chem. Soc. Rev.* **1995**, *24*, 341–350.

131. Wales, D. J.; Ulker, S. Structure and Dynamics of Spherical Crystals Characterized for the Thomson Problem. *Phys. Rev. B* **2006**, *74*, 212101.

132. Kusumaatmaja, H.; Wales, D. J. Defect Motifs for Constant Mean Curvature Surfaces. *Phys. Rev. Lett.* **2013**, *110*, 165502.

133. Yao, Z.; Olvera de la Cruz, M. Topological Defects in Flat Geometry: The Role of Density Inhomogeneity. *Phys. Rev. Lett.* **2013**, *111*, 115503.

134. Steiner, E.; Fowler, P. W. Ring Currents in Aromatic Hydrocarbons. *Int. J. Quantum Chem.* **1996**, *60*, 609–616.

135. Lee, J. *Riemannian Manifolds: An Introduction to Curvature*, 1st ed.; Graduate Texts in Mathematics 176; Springer: New York, 1997.

136. Hollerer, S.; Celigoj, C. C. Buckling Analysis of Carbon Nanotubes by a Mixed Atomistic and Continuum Model. *Comput. Mech.* **2013**, *51*, 765–789.

137. Bobenko, A. I.; Suris, Y. B., Eds. *Discrete Differential Geometry: Integrable Structure*, 1st ed.; Graduate Studies in Mathematics; American Mathematical Society: Providence, RI, 2009; Vol. 98.

138. Arroyo, M.; Belytschko, T. Nonlinear Mechanical Response and Rippling of Thick Multiwalled Carbon Nanotubes. *Phys. Rev. Lett.* **2003**, *91*, 215505.

139. Arroyo, M.; Belytschko, T. Finite Crystal Elasticity of Carbon Nanotubes Based on the Exponential Cauchy–Born Rule. *Phys. Rev. B* **2004**, *69*, 115415.

140. Erickson, J. L. On the Cauchy–Born Rule. *Math. Mech. Solids* **2008**, *13*, 199–220.

141. do Carmo, M. *Differential Geometry of Curves and Surfaces*, 1st Ed.; Prentice Hall: Englewood Cliffs, NJ, 1976.

142. Gonzalez, J.; Guinea, F.; Vozmediano, M. A. H. Continuum Approximation to Fullerene Molecules. *Phys. Rev. Lett.* **1992**, *69*, 172–175.

143. Sukumar, N.; Tabarraei, A. Conforming Polygonal Finite Elements. *Int. J. Numer. Methods Eng.* **2004**, *61*, 2045–2066.

144. Wales, D. J. *Energy Landscapes: Applications to Clusters, Biomolecules and Glasses*, 1st ed.; Cambridge University Press: Cambridge, 2004.